Wiley Online Library
Early View publication on www.wileyonlinelibrary.com
(issue and page numbers not yet assigned;
citable using Digital Object Identifier – **DOI**)

Phys. Status Solidi B, 1–6 (2014) / **DOI** 10.1002/pssb.201451010

physica status solidi b
www.pss-b.com
basic solid state physics

High-throughput evaluation in nitrogen doping of amorphous titanium dioxide

Barry J. Haycock*[,1], Gary Lander[1], M. Kylee Rice[1], Kiran Prasai[2], Binay Prasai[2†], David A. Drabold[2], and James P. Lewis*[,1]

[1] Department of Physics and Astronomy, West Virginia University, Morgantown, WV 26506-6315, USA
[2] Department of Physics and Astronomy, Ohio University, Athens, OH 45701, USA

Received 16 January 2014, revised 27 February 2014, accepted 7 March 2014
Published online 26 April 2014

Keywords *ab-initio* calculations, amorphous materials, high throughput, nitrogen doping, photocatalysis, TiO_2

* Corresponding author: e-mail barry.haycock@mail.wvu.edu, Phone: +1 304 2933435, Fax: +1 304 2933435
† Present address: Department of Physics, Central Michigan University, Mount Pleasant, MI 48859, USA.

We present an *ab-initio* investigation of the structural, electronic, and optical properties of substitutional nitrogen doping of a-TiO_2. Through observation of multiple N-doped amorphous structures, we find additional localized tail states within the band gap. Some structures show these states nearly 1 eV above the valence band, while most structures show these states very close to the valence band edge. We also observe a general trend of increasing cohesive energy with increasing distance between nitrogen impurities, suggesting the tendency for nitrogen to form localized clusters within the material.

1 Introduction Titanium dioxide has been utilized for many years in a variety of applications, including pigmentation, a protective chemical in sunscreen [1], water treatment [2], air purification [3], deodorization, and sterilization [4]. One of the most exciting attributes of TiO_2 is its photocatalytic ability. In 1972, Fujishima and Honda [5] demonstrated that TiO_2 could be used as a photocatalyst to electrochemically split water into H_2 and O_2, pioneering the solar energy conversion of materials by semiconductors. Due to their wide band gaps, both intrinsic crystalline and amorphous TiO_2 are stable against photo-corrosion, making them desirable as a material in industrial applications of this nature. However, this large band gap is also a major disadvantage of TiO_2 for photocatalysis as the activation energy is in the ultraviolet (UV 290–400 nm), which is only about 3–5% of the total radiation output of the sun. It is crucial to narrow the bandgap of TiO_2 to enable absorption of visible light frequencies and thus increase its photocatalytic activity when exposed to sunlight at the surface of the Earth.

Several different methods are used in attempts to make crystalline TiO_2 photosensitive to a larger section of the solar spectrum. Such methods include injection of noble metals onto the surface [6–8], dye photosensitization [9–12], and both cation and anion-doping of metal ions or non-metal ions into the crystal lattice [13–16]. Asahi et al. [17] showed in 2001 that doping TiO_2 with nitrogen enabled visible light absorption. Nitrogen doping helped to show that anion-doping can increase the photo-response of TiO_2 over much of the visible portion of the electromagnetic spectrum. Subsequent research has shown that non-metal anion dopants, such as carbon [18–23], sulfur [24–27], and nitrogen [3, 17, 28–34], and in some cases multiple anion co-dopants [23, 35–39], enable TiO_2 to absorb visible light by reducing the intrinsic band gap. Control of the bandgap by metal cation doping in TiO_2 is an important breakthrough, however, cation-doping in TiO_2 tends to create localized mid-gap d-states which often serve as recombination centers for the photo-generated charge carriers. Cation-doping is therefore ineffective in increasing the photo-activity of TiO_2 in the visible range [4, 40]. Through electronic density of states (DOS) calculations, Asahi et al. [17] showed that the replacement of oxygen with nitrogen is a very effective method for increasing the photo-activity of crystalline TiO_2 in the visible range. This is due to the creation of tail states from overlapping N and O 2p-orbitals at the valence band.

Amorphous TiO_2 has been less researched than its crystalline form, since it was declared to be photocatalytically inactive due to its defective states [41]. However, composite semiconductor coupling, or the layering of two or more different semiconductors [2], has been shown to make a-TiO_2 photocatalytically active by narrowing the band gap

and permitting absorption of light in the visible region. It is known that the major features in the electronic structure of amorphous and crystalline TiO_2 are qualitatively similar [4], for example in 2004, Stromme et al. [42] showed by *ab-initio* calculations that the shape of the electronic DOS in the conduction band of a-TiO_2 was in good agreement with band structure calculations for crystalline forms. Similarly, our previous calculations in a publication by Prasi et al. show the same DOS shape [43].

As compared to crystalline TiO_2, thin films of a-TiO_2 do not need thermal treatment and are less structurally dependent on the substrate materials, which is advantageous for practical applications as it simplifies the preparation process [2]. In the amorphous form, TiO_2 is easily synthesized as a thin film for industrial applications, further reducing cost of deployment as a new technology. In this paper, we present results that show nitrogen-doped a-TiO_2 to be an economically viable, stable, wide bandwidth optically excited photoreduction agent with potential application in a number of fields.

2 Computational methods We simulate substitutional nitrogen doping of a-TiO_2, and discuss the effects on its electronic and optical properties. For our simulations we use the *ab-initio* tight-binding molecular dynamics (TBMD) as implemented in the FIREBALL [4, 19] package, a self-consistent formulation of the Harris–Foulkes functional [44, 45]. This method has been successfully applied to many different systems, such as clathrate structures, zeolites, semiconducting materials, biomolecules as well as several studies on TiO_2 [23, 33, 34, 44, 46–53]. We chose a minimal basis set for N ($r_c = 3.7$, 4.1 a_B), O ($r_c = 3.4$, 3.8 a_B), and Ti ($r_c = 5.8$, 6.2, 5.4 a_B) to carry out our calculations on nitrogen doped a-TiO_2; the r_c values in the parentheses are the cutoff of the wavefunctions for s, p, and d shells, respectively. We start with a structure of a-TiO_2 which was created by random site placement and *ab-initio* simulations using the "melt-quench" method discussed in previous works [43, 54–60] where we begin by calculations of the molecular dynamics of the structure at 2200 K for 8 ps, followed by rapid cooling to 1100 K at a rate of 75 K ps^{-1}. It has been confirmed that the stoichiometry of a-TiO_2 were retained in these models [43, 58]. The unsubstituted supercell consists of 64 titanium atoms and 128 oxygen atoms in a random-yet-energetically minimized phase. In this way, we generate a supercell that is analogous to a purely amorphous structure, allowing us to explore the properties of N-substitution in this material in depth.

We study the properties at three levels of substitution; namely, the resultant material of two, four, or six O-sites randomly substituted with N. These low levels of substitution represent alloying of ~2.0, ~3.5, and ~5.0%. At these low levels of substitution, the number of permutations for possible substitution sites represents a very large search space. Therefore, 200 supercells are generated by randomly selecting substitution sites at each alloying level. For each supercell, we calculate the total energy in order to identify

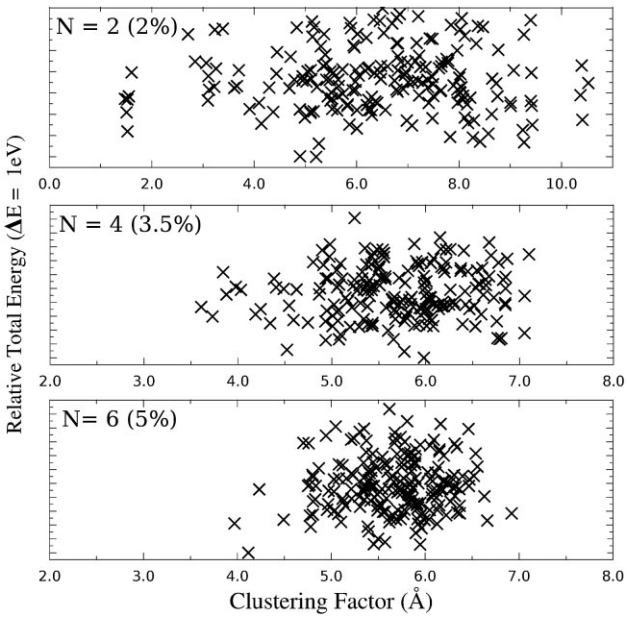

Figure 1 Clustering factor versus cohesive energy for all supercells studied. As would be expected, the range of clustering factors is broader at lower substitution levels. The lower-energy supercells, however, have a clustering factor between ~4.5 and ~6 Å.

trends in the N–N distances within the cell. The N–N distances are defined by a *clustering factor*, which measures the nearest-neighbor nitrogen distances from one another and finds the route-mean-square of these values for each nitrogen within each supercell. This value for each supercell is plotted against the cohesive energy of the cell, shown in Fig. 1 below.

Supercells with the lowest cohesive energy are selected for further investigation. We calculate the electronic properties of these systems and show that each of the low energy structures have similar properties that can be entirely predicted by our techniques and applied to laboratory studies of a-TiO_2 as photocatalyics.

3 Results

3.1 Physical metrics We first study the Clustering Factor plotted against the relative energy for each supercell and ascertain trends in this data. We define the *clustering factor* by:

$$\text{Clustering Factor} = \sqrt{\frac{\sum_{i,j}(\Delta D_{ij})^2}{n}} \qquad (1)$$

where n is the number of atoms of interest, in this case the N impurities, and $\mathbf{\Delta} D_{i,j}$ is the distance between atoms i and j. The *clustering factor* is therefore a root-mean-square of the distances between each the impurity sites and is essentially a metric defining the proximity of impurities from one another so as they can be plotted with respect to energy. The

clustering factor metric allows comparison of the properties of supercells with different levels of impurities as well as the properties of cells of equal impurity levels. Figure 1, below shows the *clustering factor* calculated for all 2-nitrogen (2N), 4-nitrogen (4N), and 6-nitrogen (6N) supercells, representing substitutional alloying of 2%, 3.5%, and 5%, respectively.

The first important observation that can be made about the *clustering factor* versus cohesive energy plots in Fig. 1 is that the RMS of the N–N distance in all regimes studied is about 5.0 Å or tending toward that value for the low-energy structures. The immediate implication of a *clustering factor* of ∼5.0 Å is that it is well above the molecular N_2 triple-covalent-bond distance of approximately 1.3 Å. The fact that the N atoms prefer to maintain that distance from one another means that the supercells do not contain grains of nitrogen within the a-TiO_2 structure. In the 2N case, there are some supercells with relatively low energy and a *clustering factor* of 1.5 Å, implying that some lower-energy structures are forming N–N bonds, but not necessarily the molecular N_2 bonds. The low *clustering factor* configurations in the 2N supercells have a cohesive energy that is >1.5 eV above the lowest energy structures, and we conclude that they are therefore energetically unfavorable N configurations within the supercell.

There is a very strong agreement of *clustering factor* of between 4.5 and 6.0 Å for the low-energy configurations. The low range of *clustering factor* for low cohesive energy structures suggests that the N atoms prefer to occupy sites that are not adjacent. The *clustering factor* plots in Fig. 1 show that there is a tendency for the nitrogen atoms to keep a certain distance from one another. However, when individual supercells are inspected we occasionally observe small groups of N atoms which allow for the N atoms maximize the overall RMS distance from one another such that the overall average distance is still about 5 Å. By inspection of the lowest energy supercells we find that at the 2N and 4N levels the N atoms succeed in finding a maximal distance from one another, but at the 6N level there is a necessity for the N atoms to be somewhat closer to one another in small groups, these "pockets" of N atoms close to one another allows for greater overall clustering factor as these groups maximize their distance from each other. We suspect that the low energy configurations found are due to a balance of forces so as to maximize the average N–N distances at the 6N level.

3.2 Electronic calculations The lower-energy structures in each alloying regime are selected and the partial density-of-states (PDOS) and W is calculated for each structure. This information is plotted, allowing for trends in lower energy structures to be seen more clearly.

The partial density of stated (PDOS) is shown with a similar breakdown by doping regime and comparison to the undoped structures is shown in Figs. 2 and 3.

Inspection of Figs. 2 and 3 reveal that the band gap is, generally, about the same in all cases, however, the relative energies of the bands vary between structures, as would be expected in amorphous materials. The DOS of the 5% case in Fig. 2 shows small peaks in the gap, which are shown for one case in the PDOS in Fig. 3, revealing those peaks to be due to the presence of nitrogen.

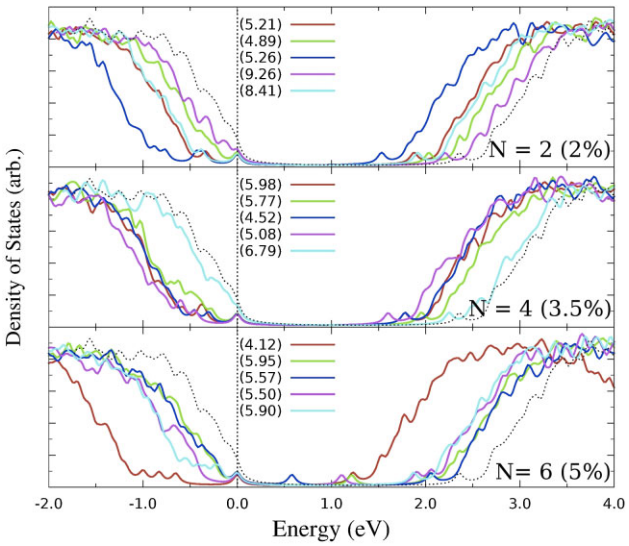

Figure 2 Calculated total density of states for each of the lower-energy structures found for each doping regime. The vertical dotted line represents the HOMO band edge, the dotted-line plot represents the calculated DOS for undoped a-TiO_2. The corresponding clustering factor for each structure plotted is in brackets in the legend.

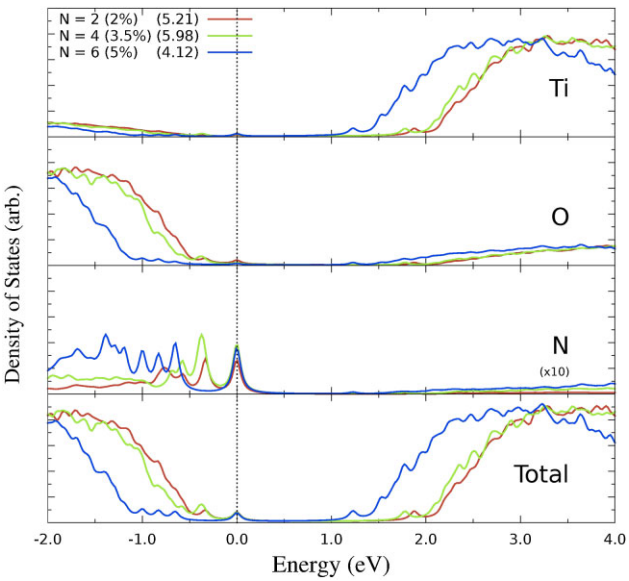

Figure 3 Calculated partial density-of-states (PDOS) for the lowest-energy reconstruction for each doping regime studied. The dotted vertical line represents the HOMO band edge, the dotted-line plot represents the PDOS for undoped a-TiO_2.

To quantify the effects of doping concentration on the photoresponse, we calculate the extent of localization for electronic states near the band edge. We use the W-parameter, which gives the number of accessible atoms in a particular electronic state and describes the spatial extent of this state [61]. For a particular state ν, the wavefunction $\varphi(\nu)$ has a Mulliken population $p_i(\nu)$ on atom i, which loosely is considered the probability that an electron is in state ν and resides on particular atom i. From probability theory, we define an information entropy for state ν as $S(\nu) = -\sum_i p_i(\nu) \ln[p_i(\nu)]$ with the populations normalized, $\sum_i p_i(\nu) = 1$. From Boltzmann's equation, we can determine the number of accessible atoms $W(\nu)$ for a given electronic state $W(\nu) = \exp[S(\nu)]$. The number of accessible atoms $W(\nu)$ gives a quantitative, and easily calculable, measure of how many atom sites a particular electronic state $\varphi(\nu)$ resides at. We plot the result of this analysis in Fig. 4, where we compare the lower-energy structures found in each alloying regime, and the results of an undoped supercell in comparison with one supercell from each of those regimes.

The plots shown in Fig. 4 show that the very dispersed state at 2.2 eV above the HOMO in the undoped structure is only ~1 to ~1.5 eV above the HOMO in the presence of nitrogen. The electronic structure of the intrinsic a-TiO_2 proved to be interesting on its own account. Urbach tails [60], which are exponential falloffs of the number of accessible atoms at the edges of the band gap, are apparent on the valence band edge. In all cases, there is a highly delocalized state on the conduction band edge that is due to the titanium and is a property of amorphous TiO_2, as it is also present in the intrinsic structure. In 2011, Cai and Drabold [56] produced similar results for the electronic structure of amorphous GaN. There they saw Urbach tails on the valence band edge with the conduction band edge very delocalized. This is in agreement with our results and we believe this is a property of amorphous binary systems since this is not seen in amorphous single element structures, such as amorphous silicon [54, 62].

A highly dispersed conduction band edge is shown in all cases in Fig. 4. Comparison of Figs. 2 and 4 shows that the highly dispersed conduction band edge is centered on the titanium atoms. In the case of the 5% alloyed structures, the nitrogen-based peaks from the DOS are highly localized states within the gap.

In the doped structures, the substituted nitrogen produces states within the band gap, but the exact location and localization of these states differ amongst the lowest energy structures. Out of the structures considered, most had nitrogen atoms that did not get close enough to form N_2 bonds, in which we observed introduced tail states very close to the valence band edge. The localization of these states often did not differ much from the localization of the edge of the valence band of the intrinsic amorphous TiO_2 structure. Although the localization of these tail states never significantly increased when compared to the localization of the valence band edge of the intrinsic a-TiO_2, in a few cases

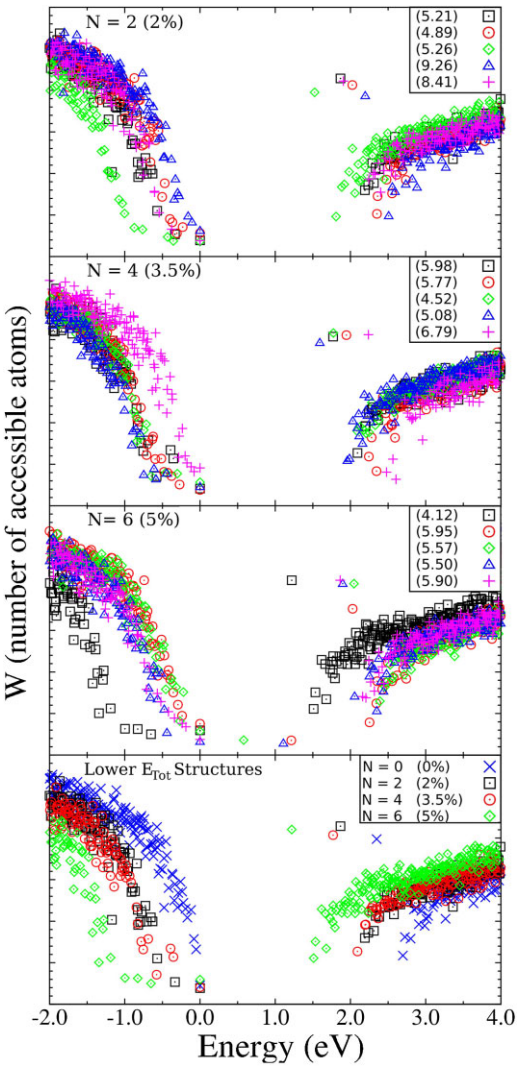

Figure 4 The W-plots calculated for the lower-energy supercells found in this study. (All plots are offset in energy such that zero is the HOMO band edge.) Comparison with the PDOS plots shows that the highly-dispersed states in the LUMO are Ti-based, whereas the LUMO tails into the gap (Urbach tails) originate due to N states. The bottom-right image shows the lowest-energy reconstruction in each regime with the W-plot of the undoped structure for direct comparison.

the created tail states where actually more de-localized than the valence band edge of the undoped a-TiO_2. The nitrogen states allow for there to be more available electrons to be excited to the conduction band via visible light absorption. If the electrons from such localized states are excited to the conduction band, it would be consistent with the absorption edge shifting to lower energies [63]. Thus, in all cases where N_2 bonds were not formed, we see a narrowing of the band gap via the creation of tail states that are close enough to the valence band edge that we expect them to not act as recombination centers for the charge carriers. Consequently, we can assume that the photocatalytic activity of a-TiO_2 is

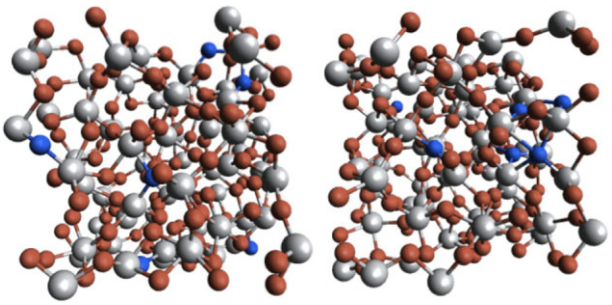

Figure 5 Example supercells from the 6N (5%) N-doped a-TiO_2 supercells. The left image shows no examples of N–N bond formation, whereas the right supercells show a clustering of N atoms.

increased via nitrogen doping as long as N_2 states are not formed.

As N increases, chances of N–N bonds also increase as there are less sites available that are a large distance from all other N-filled sites as the amount of N in the supercell increases. Peaks in 5% DOS appear indicative of N–N bond formation, and inspection of the N placement in the supercell confirm such a configuration. Figure 5 shows the 5% supercells with examples of N–N bond cases and "no N–N bond" cases. In such cases, including higher energy structures, fairly localized N_2 states were created within the band gap isolated from the valence band edge. Such states so close to the middle of the band gap will act as recombination centers for the conduction electrons and holes, thus creating an unsuitable photocatalyst.

However, as mentioned previously, we do not see Urbach tails on the edge of the conduction band but do see a very highly de-localized state on the conduction band edge in both the intrinsic and N-doped a-TiO_2. Other than a slight decrease in the size of the gap, we see that the conduction band edge seems to be unchanged, or changed insignificantly, when the substituted nitrogen is introduced which indicates that the nitrogen-doped a-TiO_2 satisfies the requirement for obtaining a versatile photocatalytic material.

4 Conclusions We expect that the photoactivity of a-TiO_2 is enhanced by substitutional nitrogen doping, which introduces tail states near the valence band edge. However, in the couple cases when N_2 is formed within the structure, we see the introduction of localized, isolated states near the middle of the band gap that we believe will most likely serve as recombination centers for the charge carriers. We observe a general trend of increasing cohesive energy with increasing N–N separation distance although the very lowest energy structures had N–N separation distances around 4.5 Å, in contrast to the smallest seen N–N separation distances of around 1.5 Å. Urbach tails on the valence band and a very highly de-localized state on the conduction band edge were seen and are believed to be a property of amorphous binary materials. We see an increase in the likelihood of N_2 bond formation as the level of N impurities increases. When N_2 bonds are not formed, the introduced tail states will narrow the band gap while not acting as recombination centers for the charge carriers, thus promoting absorption in the visible spectrum and increasing the photocatalytic activity of amorphous TiO_2.

Acknowledgements The National Science Foundation sponsored this research through NSF DMR 09-03225. Additionally, DAD thanks for Army Research Office for support.

References

[1] J. Winkler, Titanium Dioxide (Vincentz Network, Hannover, 2003).
[2] J. M. Huang, Y. Liu, L. Lu, and L. Li, Res. Chem. Intermed. **38**(2), 487–498 (2012).
[3] X. K. Li, Z. Zhuang, W. Li, and H. Pan, Appl. Catal. A **429–430**, 31–38 (2012).
[4] H. Wang and J. P. Lewis, J. Phys.: Condens. Matter **18**(2), 421–434 (2006).
[5] A. Fujishima and K. Honda, Nature **238**(5358), 269–271 (1972).
[6] H. M. Sung-Suh et al., J. Photochem. Photobiol. A **163**(1–2), 37–44 (2004).
[7] X. F. You et al., Catal. Lett. **102**(3–4), 247–250 (2005).
[8] H. Y. Chuang and D. H. Chen, Nanotechnology **20**(10), 105704 (2009).
[9] C. Wang et al., Appl. Catal. B **76**(3–4), 218–226 (2007).
[10] G. Mele et al., J. Catal. **217**(2), 334–342 (2003).
[11] T. V. Nguyen, J. C. S. Wu, and C. H. Chiou, Catal. Commun. **9**(10), 2073–2076 (2008).
[12] Y. X. Li et al., Int. J. Hydrogen Energy **34**(14), 5629–5636 (2009).
[13] D. Chatterjee and S. Dasgupta, J. Photochem. Photobiol. C **6**(2–3), 186–205 (2005).
[14] H. Yamashita et al., J. Phys. Chem. B **102**(52), 10707–10711 (1998).
[15] W. Y. Su et al., Langmuir **24**(7), 3422 (2008).
[16] A. Di Paola et al., J. Phys. Chem. B **106**(3), 637–6345 (2002).
[17] R. Asahi et al., Science **293**(5528), 269–271 (2001).
[18] K. Noworyta and J. Augustynski, Electrochem. Solid-State Lett. **7**(6), E31–E33 (2004).
[19] H. Wang and J. P. Lewis, J. Phys.: Condens. Matter, **17**(21), L209–L213 (2005).
[20] X. X. Zou et al., Int. J. Photoenergy **2012**, 720183 (2012).
[21] E. Kusiak-Nejman et al., J. Photochem. Photobiol. A **226**(1), 68–72 (2011).
[22] Q. Xiao et al., Sol. Energy **82**(8), 706–713 (2008).
[23] H. Wang and J. P. Lewis, J. Phys.: Condens. Matter **17**(21), L209–L213 (2005).
[24] T. Umebayaski et al., Appl. Phys. Lett. **81**(3), 454–456 (2002).
[25] T. Umebayaski et al., Chem. Lett. **32**(4), 330–331 (2003).
[26] T. Yamamoto et al., Mater. Trans. **45**(7), 1987–1990 (2004).
[27] T. Umebayashi et al., J. Appl. Phys. **93**(9), 5156–5160 (2003).
[28] D. G. F. David et al., J. Cryst. Growth **350**(1), 11–16 (2012).
[29] M. C. Wang et al., Ceram. Int. **38**(1), 195–200 (2012).
[30] Y. C. Tang et al., Int. J. Photoenergy **2012**, 960726 (2012).
[31] R. Asahi et al., Science **293**(5528), 269–271 (2001).
[32] P. Reeves et al., Sol. Energy **48**(6), 413–420 (1992).

[33] D. N. Tafen et al., Appl. Phys. Lett. **94**(9), 093101 (2009).
[34] J. Wang et al., J. Am. Chem. Soc. **131**(34), 12290–12297 (2009).
[35] X. W. Cheng, X. J. Yu, and Z. P. Xing, J. Colloid Interface Sci. **372**, 1–5 (2012).
[36] X. W. Cheng, X. J. Yu, and Z. P. Xing, Appl. Surf. Sci. **258**(19), 7644–7650 (2012).
[37] Y. F. Ma et al., Microporous Mesoporous Mater. **156**, 145–152 (2012).
[38] M. Hamadanian et al., Appl. Surf. Sci. **257**(24), 10639–10644 (2011).
[39] P. H. Wang, P. S. Yap, and T. T. Lim, Appl. Catal. A **399**(1–2), 252–261 (2011).
[40] O. Diwald et al., J. Phys. Chem. B **108**(19), 6004–6008 (2004).
[41] M. Nakamura et al., J. Mater. Res. **16**(2), 621–626 (2001).
[42] M. Stromme, R. Ahuja, and G. A. Niklasson, Phys. Rev. Lett. **93**(20), 206403 (2004).
[43] B. Prasai et al., MS&T-11 Conf. Proceedings (2011).
[44] A. A. Demkov et al., Phys. Rev. B **52**(3), 1618–1630 (1995).
[45] W. M. C. Foulkes, in: Atomistic Simluation of Materials: Beyond Pair Potentials, edited by V. Vitek et al. (Plenum Press, New York, 1989), pp. 353–359.
[46] J. P. Lewis et al., Phys. Rev. B **64**(19), 195103 (2001).
[47] G. B. Adams et al., Phys. Rev. B **49**(12), 8048–8053 (1994).
[48] H. Wang, J. P. Lewis, and O. F. Sankey, Phys. Rev. Lett. **93**(1), 016401 (2004).
[49] O. F. Sankey et al., Int. J. Quantum Chem. **69**(3), 327–340 (1998).
[50] N. Wu et al., J. Am. Chem. Soc. **132**(19), 6679–6685 (2010).
[51] D. N. Tafen and J. P. Lewis, Phys. Rev. **80**(1), 014104 (2009).
[52] J. B. Keith et al., J. Phys.: Condens. Matter **20**(2), 022202 (2008).
[53] H. Wang and J. P. Lewis, J. Phys.: Condens. Matter, **18**(2), 421–434 (2006).
[54] T. A. Abtew, M. L. Zhang, and D. A. Drabold, Phys. Rev. B **76**(4), 045212 (2007).
[55] R. Atta-Fynn et al., Phys. Rev. B **69**(8), 085207 (2004).
[56] B. Cai and D. A. Drabold, Phys. Rev. B **84**(7), 075216 (2011).
[57] D. A. Drabold, P. Biswas, D. Tafen, and R. Atta-Fynn, in: Non-Crystalline Materials for Optoelectronics, edited by M. Popescu (INOE, Bucharest, 2004), pp. 441–467.
[58] D. A. Drabold, Eur. Phys. J. B, Condens. Matter Complex Syst. **68**(1), 1–21 (2009).
[59] J. P. Lewis, P. Jelinek, J. Ortega, A. A. Demkov, D. G. Trabada, B. Haycock, H. Wang, G. Adams, J. K. Tomfohr, E. Abad, H. Wang, and D. A. Drabold, Phys. Status Solidi B **248**(9), 1989–2007 (2011).
[60] Y. Pan et al., Phys. Rev. Lett. **100**(20), 206403 (2008).
[61] P. Lewis et al., J. Phys. Chem. B **107**(11), 2581–2587 (2003).
[62] T. A. Abtew and D. A. Drabold, J. Phys.: Condens. Matter **18**(1), L1–L6 (2005).
[63] N. Serpone, J. Phys. Chem. B **110**(48), 24287–24293 (2006).

